Collaborative Magnetic Manipulation via Two Robotically Actuated Permanent Magnets

Giovanni Pittiglio, *Member, IEEE,* Michael Brockdorff, Tomas da Veiga, Joshua Davy, James H. Chandler, *Member, IEEE,* and Pietro Valdastri, *Fellow, IEEE*

***Abstract*— Magnetically actuated robots have proven effective in several applications, specifically in medicine. However, generating high actuating fields with a high degree of manipulability is still a challenge, especially when the application needs a large workspace to suitably cover a patient. The presented work discusses a novel approach for the control of magnetic field and field gradients using two robotically actuated permanent magnets. In this case, permanent magnets - relative to coil-based systems - have the advantage of larger field density without energy consumption. We demonstrate that collaborative manipulation of the two permanent magnets can introduce up to three additional Degrees of Freedom (DOFs) when compared to single permanent magnet approaches (five DOFs). We characterized the dual-arm system through the measurement of the fields and gradients, and show accurate open loop control with 13.5% mean error. We then demonstrate how the magnetic DOFs can be employed in magneto-mechanical manipulation, by controlling and measuring the wrench on two orthogonal magnets within the workspace, observing a maximum cross-talk of 6.1% and mean error of 11.1%.**

***Index Terms*— Force Control, Medical Robots and Systems, Formal Methods in Robotics and Automation, Magnetic Actuation.**

I. Introduction

Magnetic actuation is capable of applying force and torque remotely, and has recently been introduced for several applications in medical robotics. Remote actuation capabilities facilitate miniaturization, which is particularly desirable for minimally invasive diagnosis and treatment in the human body. However, current approaches to magnetic actuation are typically limited by either a reduced workspace or potential to control a restricted number of DOFs. Herein, we present and fully characterize the dual External Permanent Magnet (dEPM) platform, which has the potential to overcome both limitations. It is characterized by a large workspace and can generate *gradient-free fields* in three dimensions and up to five independent magnetic field *gradients*.

Whilst the platform can be applied to magnetic robots, spanning nano-, micro- and milli-meter scale, we mainly focus of the latter. Millimeter scale magnetic actuation poses several challenges, related to the generated uniform fields in a larger workspace and the requirement of higher actuating wrenches (forces and torques), thus higher field strengths. While successful multi-DOFs magnetic actuation has been demonstrated at small scale [1], [2], [3], [4], [5], [6], by using systems of *coils*, large-scale (milli- to centi-meter) manipulation is yet to be fully proven. In fact, it might require several independently-controlled coils [7], [8], [9] to be effective along any possible direction of motion. Despite their ability to generate both homogeneous fields [10] and gradients [5], [7], [11], systems of coils are less scalable, compared to permanent magnet-based magnetic actuators [12], [10], [13]. In fact, to generate high fields via coil-based systems requires high power and can necessitate high-performance cooling systems. In many cases, designs are therefore restricted to a limited workspace [14], [15]. However, a main advantage of coil-based actuation comes from the possibility to readily generate linear field change, which is difficult to produce with permanent magnet based systems.

Systems of rotating permanent magnets have been proposed to mitigate energy consumption [16], but large scale actuation is yet to be demonstrated.

Large scale actuation systems include usage of dual-External Permanent Magnets (EPMs) [17], the coil actuation systems presented in [18], [19], [20], [21] as well as the use of MRIs for both actuation and intraoperative imaging. The former is in use for actuation of magnetic cardiovascular catheters, but only field actuation has been considered, so far, while we consider the control of fields and gradients independently. By considering that the EPMs can move asymmetrically with respect to each other, we contrast the idea of minimizing gradients [22], [23]. Both the gradient coils within an MRI [24], [25] and the fringe field created by the MRI bore magnet [26] have been shown to be suitable magnetic actuators. However, these systems have not yet been proven effective for multi-magnet manipulation. Although multi-magnet actuation techniques have been proposed, such systems are either characterized by

Research reported in this article was supported by the Royal Society, by the Engineering and Physical Sciences Research Council (EPSRC) under grant number EP/R045291/1, and by the European Research Council (ERC) under the European Union's Horizon 2020 research and innovation programme (grant agreement No 818045). Any opinions, findings and conclusions, or recommendations expressed in this article are those of the authors and do not necessarily reflect the views of the Royal Society, EPSRC, or the ERC.

Giovanni Pittiglio is with the Department of Cardiovascular Surgery, Boston Children's Hospital, Harvard Medical School, Boston, MA 02115, USA and with the STORM Lab, Institute of Autonomous Systems and Sensing (IRASS), School of Electronic and Electrical Engineering, University of Leeds, Leeds, UK. Email: giovanni.pittiglio@childrens.harvard.edu

Michael Brockdorff, Tomas da Veiga, Joshua Davy, James H. Chandler, and Pietro Valdastri are with the STORM Lab, Institute of Autonomous Systems and Sensing (IRASS), School of Electronic and Electrical Engineering, University of Leeds, Leeds, UK. Email: {elmbr, eltgdv, el17jd, j.h.chandler, p.valdastri}@leeds.ac.uk

workspace constraints [14] or exhibit low controllability [27] compared to the findings discussed in this paper. By further developing on the idea of remotely actuating a single Internal Permanent Magnet (IPM) (internal since, generally, inside the human body) with a single EPM [12], we discuss how a pair robotically actuated EPMs are able to magnetically manipulate two IPMs, independently. This is achieved by independently controlling the torque (correlated to magnetic field) and the force (correlated to field gradients) applied to each IPM.

In the present work, we assume the field generated by the two EPMs can be approximated with the dipole model and that the superposition principle applies. This is the case when the EPMs are far enough from the point of interest [28] and the workspace is free from metallic objects, which could deflect the field. We, first, introduce the concept of magnetic actuation and discuss the maximum controllable DOFs in a point. Then, we analyse the case of multi-point magnetic manipulation and provide a numerical analysis of the independent magnetic DOFs controllable in a large workspace.

Finally, we focus on robotic control of two EPMs and discuss *magnetic manipulability*, i.e. the ability of the robotic platform to generate combinations of independent fields and gradients. We validate our results by analysing the fields and gradients generated by the platform by using a teslameter. We also prove that we can control up to eight magneto-mechanical DOFs by measuring the generated wrench on two IPMs by means of high-resolution load cells.

II. Magnetic Actuation

In the following, we describe the concept of multi-DOF magnetic manipulation. Specifically, we introduce the components of field and gradients that can be independently controlled.

We consider the case of actuating magnetic fields and gradients in a specified workspace $\mathcal{W} \equiv \{O,\ x,\ y,\ z\}$, with origin O and principal axes $x,\ y,\ z$, as indicated in Fig. 1. From here on, unless specified, all variables are written in the frame $\mathcal{W}$ and avoid the reference ${}^{\mathcal{W}}\cdot$.

The general field at any point p can be expressed as [10]

$$B(p) = B_0 + \frac{\partial B(p)}{\partial p}p + o(p) \approx B_0 + \frac{\partial B(p)}{\partial p}p, \quad (1)$$

with B_0 field in the origin of $\mathcal{W}$. The term $o(p)$, $\lim_{||p||\to 0} o(p) = 0$ groups the terms of order higher than one. In Section V, we quantify the linearity of the generated fields to validate our assumption. By neglecting higher order terms, the EPMs are considered as dipole sources. Although this reduces the fidelity of the model, it allows simplification when considering a small workspace. In the presented work, we consider the case of actuating two IPMs with minimal separation. This represents the worst case scenario for determination of controllable magnetic DOFs; as with increased distance between IPMs the number of magnetic DOFs that can be controlled will only increase. In Section V, we quantify the linearity of the generated fields to validate this assumption.

The matrix

$$\frac{\partial B(p)}{\partial p} \in \mathbb{R}^{3\times 3}$$

can be seen as the codistribution collection of each gradient, i.e.

$$\frac{\partial B(p)}{\partial p} = \begin{pmatrix} \frac{\partial B_x}{\partial p} \\ \frac{\partial B_y}{\partial p} \\ \frac{\partial B_z}{\partial p} \end{pmatrix} = \begin{pmatrix} \frac{\partial B_x}{\partial x} & \frac{\partial B_x}{\partial y} & \frac{\partial B_x}{\partial z} \\ \frac{\partial B_y}{\partial x} & \frac{\partial B_y}{\partial y} & \frac{\partial B_y}{\partial z} \\ \frac{\partial B_z}{\partial x} & \frac{\partial B_z}{\partial y} & \frac{\partial B_z}{\partial z} \end{pmatrix}$$

or, equivalently, as the Jacobian matrix of B at the point p. We will consider the former definition, since mostly used in literature. We assume that our workspace is free of currents, thus,

$$\begin{aligned} \nabla \cdot B &= 0 \\ \nabla \times B &= 0. \end{aligned}$$

Consequently, the matrix $\partial B(p)/\partial p$ must be symmetric and zero trace,

$$\frac{\partial B(p)}{\partial p} = \begin{pmatrix} \frac{\partial B_x}{\partial x} & \frac{\partial B_x}{\partial y} & \frac{\partial B_x}{\partial z} \\ \frac{\partial B_x}{\partial y} & \frac{\partial B_y}{\partial y} & \frac{\partial B_y}{\partial z} \\ \frac{\partial B_x}{\partial z} & \frac{\partial B_y}{\partial z} & -\frac{\partial B_x}{\partial x} - \frac{\partial B_y}{\partial y} \end{pmatrix}$$

and the five independent components of the gradients can be collected in the vector field

$$\mathrm{d}B(p) = \left(\frac{\partial B_x(p)}{\partial x} \ \frac{\partial B_x(p)}{\partial y} \ \frac{\partial B_x(p)}{\partial z} \ \frac{\partial B_y(p)}{\partial y} \ \frac{\partial B_y(p)}{\partial z} \right)^T.$$

We will refer to $\cdot^* : \mathbb{R}^5 \to \mathbb{R}^{3\times 3}$ as the mapping from the independent components of the gradients to the gradients codistribution: $\mathrm{d}B^*(p) = \frac{\partial B(p)}{\partial p}$.

III. Magneto-Mechanical Manipulation

The magnetic actuation paradigm presented here targets mechanical manipulation. Specifically, we aim to translate the magnetic work into mechanical work, to facilitate remote manipulation of *magnetic agent(s)*. A magnetic agent is here referred to as a body, either locally rigid or flexible, characterized by an intrinsic magnetization; they can be permanent magnet-based or electrically actuated coils. We can describe the magnetization of the ith agent with its global *magnetic dipole* vector ${}^{\mathcal{W}}m_i \in \mathbb{R}^3$ or m_i, for simplicity's sake.

Each agent is also characterized by a specific and, generally time-dependent, location ${}^{\mathcal{W}}p_i \equiv p_i \in \mathbb{R}^3$. Thus, when the actuation system applies a field B_0 and gradients $\mathrm{d}B_0$ at the origin of $\mathcal{W}$, the ith agent experiences the gradients $\mathrm{d}B_0$ and a field following (1),

$$\begin{cases} \mathrm{d}B(p_i) &= \mathrm{d}B_0 \\ B(p_i) &= B_0 + \mathrm{d}B_0^* p_i \end{cases}.$$

Consequent to its magnetic dipole m_i and location p_i within a field, the agent would experience a wrench

$$w_i = \begin{pmatrix} f_i \\ \tau_i \end{pmatrix} = \begin{pmatrix} \mathrm{d}B^*(p_i)\ m_i \\ m_i \times B(p_i) \end{pmatrix}, \quad (2)$$

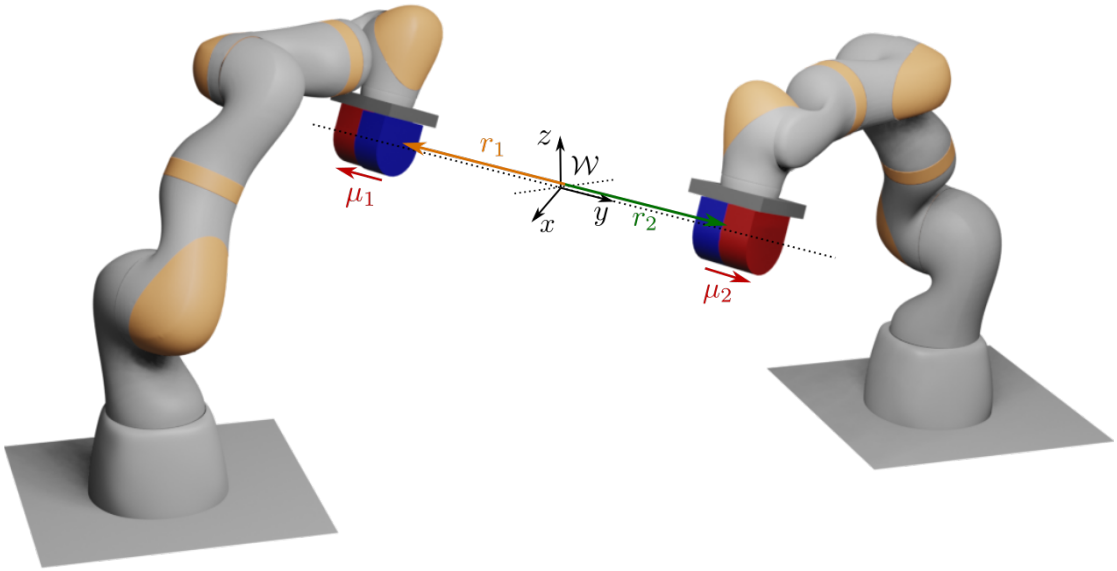

Fig. 1: Schematic representation of the dEPM platform.

f_i and τ_i refer to the force and torque on the agent i, respectively.

To rearrange the field-wrench relationship to be linear with respect to the field and gradients [29], we introduce the operator $\cdot_+ : \mathbb{R}^3 \to \mathbb{R}^{3\times5}$ which rearranges any vector $v \in \mathbb{R}^3$, pre-multiplied by the gradients so that the multiplication commutes as

$$\mathrm{d}B^*\ v = v_+\ \mathrm{d}B.$$

Since

$$\mathrm{d}B^*v = (\mathrm{d}B_1E_{11}+\mathrm{d}B_2E_{12}+\mathrm{d}B_3E_{13}+\mathrm{d}B_4E_{22}+\mathrm{d}B_5E_{23})v$$

with $E_{ij} = e_ie_j^T + e_je_i^T$ and $E_{ii} = e_ie_i^T$, we can rearrange to

$$\mathrm{d}B^*v = (E_{11}v|\ E_{12}v|\ E_{13}v|\ E_{22}v|\ E_{23}v)\,\mathrm{d}B = v_+\mathrm{d}B.$$

The vector e_i is here referred to as the ith element of the canonical basis of $\mathbb{R}^3$. We also introduce the operator $\cdot_\times : \mathbb{R}^3 \to \mathbb{R}^{3\times3}$ as $v_\times = (v \times e_1|\ v \times e_2|\ v \times e_3)$.

Eventually, (2) can be written as

$$w_i = \begin{pmatrix} 0_{3,3} & m_{i_+} \\ m_{i_\times} & 0_{3,5} \end{pmatrix} \begin{pmatrix} B(p) \\ \mathrm{d}B(p) \end{pmatrix}. \tag{3}$$

We can rewrite (1) as

$$B(p) = B_0 + p_+\mathrm{d}B_0 \tag{4}$$

and, since $\mathrm{d}B_0 = \mathrm{d}B(p)$, due to homogeneity assumption,

$$U(p) = \begin{pmatrix} B(p) \\ \mathrm{d}B(p) \end{pmatrix} = \begin{pmatrix} I & p_+ \\ 0 & I \end{pmatrix} U_0. \tag{5}$$

We combine (5) with (3), and obtain the wrench on the ith agent of magnetic dipole m_i in a point p_i

$$\begin{aligned} w_i &= \begin{pmatrix} 0_{3,3} & m_{i_+} \\ m_{i_\times} & 0_{3,5} \end{pmatrix} \begin{pmatrix} I & p_{i_+} \\ 0 & I \end{pmatrix} U_0 \\ &= P(m_i)V(p_i)U_0 \\ &= S(p_i, m_i)U_0 \\ &= S_iU_0. \end{aligned} \tag{6}$$

To simplify the dissertation, we will focus on permanent magnets and refer to the magnetic agents as IPMs; however, the following applies to any object which may manifest a magnetic behaviour, such as coils.

As known, we can actuate a maximum five DOFs for one IPM, as $\mathrm{rank}\{S_i\} = 5$. It can also be noticed that the maximum number of magneto-mechanical DOFs we can actuate in a point is eight, as discussed in [5], [12].

Consider the wrench applied to two IPMs

$$w = \begin{pmatrix} w_1 \\ w_2 \end{pmatrix} = \begin{pmatrix} P(m_1)V(p_1) \\ P(m_2)V(p_2) \end{pmatrix} U_0 = \begin{pmatrix} S_1 \\ S_2 \end{pmatrix} U_0.$$

First, we can see that $\mathrm{rank}\{S_i\} = \mathrm{rank}\{P(m_i)\},\ \forall p_i,\ i$, since $V(p_i)$ is always full-rank. We can then consider the case $p_1 = p_2 = p_0$, as general. It is easy to notice that if m_1 and m_2 are parallel, we can control up to five DOFs, as in the single magnet case. In the case m_1 and m_2 are not parallel, we can decompose m_2 in the parallel and orthogonal component to m_1, i.e. $m_2 = m_{2_\perp} + m_{2_\parallel} = m_{2_\perp} + \lambda m_1$ for some $\lambda \in \mathbb{R}$ and rewrite the wrench as

$$w = \begin{pmatrix} S_1 \\ S_{2_\perp} + \lambda S_1 \end{pmatrix} U_0.$$

Since

$$\mathrm{rank}\left\{\begin{pmatrix} S_1 \\ S_{2_\perp} + \lambda S_1 \end{pmatrix}\right\} = \mathrm{rank}\left\{\begin{pmatrix} S_1 \\ S_{2_\perp} \end{pmatrix}\right\}$$

and being norm-independent, i.e. for any vectors of non-zero norm $m_1,\ m_2$ the rank of $S_\perp = \left(S_1^T\ S_{2_\perp}^T\right)^T$ is invariant, we can arbitrarily choose $m_1 = e_1,\ m_2 = e_2$.

To find the rank of $S_\perp$, we need to investigate the independent vectors between $m_{1_\times}$ and $m_{2_\times}$, and the independent vectors between m_{1_+} and m_{2_+}. We can compute

$$\begin{aligned} m_{1_\times} &= (e_1 \times e_1 \ |e_1 \times e_2 \ |e_1 \times e_3) = (0 \ |e_3 \ | -e_2) \\ m_{2_\times} &= (e_2 \times e_1 \ |e_2 \times e_2 \ |e_2 \times e_3) = (-e_3 \ |0 \ |e_1)\,. \end{aligned}$$

Between $m_{1_\times}$ and $m_{2_\times}$ we can find three independent vectors

$$\{-u_6,\ u_3,\ u_4 - u_2\}\,,$$

with $u_i \in \mathbb{R}^6$ ith element of the canonical bases of $\mathbb{R}^6$.

Equivalently, we analyse m_{1_+} and m_{2_+},

$$\begin{aligned} m_{1_+} &= (E_{11}e_1 \ |E_{12}e_1 \ |E_{13}e_1 \ |E_{22}e_1 \ |E_{23}e_1) \\ &= (e_1 \ |e_2 \ |e_3 \ |0 \ |0) \\ m_{2_+} &= (E_{11}e_2 \ |E_{12}e_2 \ |E_{13}e_2 \ |E_{22}e_2 \ |E_{23}e_2) \\ &= (0 \ |e_1 \ |0 \ |e_2 \ |e_3)\,, \end{aligned}$$

and find five independent vectors

$$\{u_1,\ u_2 + u_6,\ u_3,\ u_7,\ u_8\}\,.$$

Overall, this demonstrates that two magnets with non-parallel magnetic dipole direction can be actuated in eight independent DOFs anywhere in the workspace. In fact,

$$\begin{aligned} \text{rank}\left\{\begin{pmatrix} S_1 \\ S_{2_\perp} \end{pmatrix}\right\} &= \text{rank}\left\{\begin{pmatrix} m_{1_\times} \\ m_{2_\times} \end{pmatrix}\right\} \\ &\quad + \text{rank}\left\{\begin{pmatrix} m_{1_+} \\ m_{2_+} \end{pmatrix}\right\} \\ &= \text{rank}\left\{\begin{pmatrix} -u_6 & u_3 & u_4 - u_2 \end{pmatrix}\right\} \\ &\quad + \text{rank}\left\{\begin{pmatrix} u_1 & u_2 + u_6 & u_3 & u_7 & u_8 \end{pmatrix}\right\} \end{aligned}$$

thus

$$\text{rank}\left\{\begin{pmatrix} S_1 \\ S_{2_\perp} \end{pmatrix}\right\} = 8$$

Notice that this holds when they experience the same gradient thus, generally, when they are close enough. When the agents are far (i.e. the gradient is not constant), up to nine magnetic DOFs could be actuated. The further DOF, however, depends on the IPM-IPM distance and can undergo singularity issues when the magnets are in close proximity. The present paper has the aim of discussing the non-singular DOFs and does not analyze the case of the additional DOF, leaving this to future application-specific work.

It can also be noticed that adding further IPMs, in the case under analysis, would not introduce independent DOFs, since $U_0 \in \mathbb{R}^8$ and no further independent inputs can be controlled.

IV. Dual-EPM Actuation

In the present paper, we describe collaborative magnetic manipulation based on two KUKA LBR iiwa14 robots (KUKA, Germany) manipulating two cylindrical axially magnetized N52 EPMs (101.6 mm diameter and length). The pose of any permanent magnet can be related to field and gradients they generate by means of the *dipole model*. This model is accurate when the distance between the permanent magnet and the point of actuation is large enough [28]; for the EPMs considered the error is lower than 2% when the distance is larger than the magnet's radius. Our aim is to invert this relationship and find the target pose of the EPMs that generates a desired magnetic field and/or gradients.

We describe the field generated by one of the pair of EPMs as

$$B_i(r_i, \mu_i) = \frac{\mu_0 |\mu_i|}{4\pi |r_i|^3} \left(3\hat{r}_i \hat{r}_i^T - I\right) \hat{\mu}_i. \tag{7}$$

Herein, $r_i \in \mathbb{R}^3$ and $\mu_i \in \mathbb{R}^3$ are the respective position and dipole moment of the EPM with respect to the workspace center; $|\cdot|$ stands for the Euclidean norm, $\hat{\cdot} = \frac{\cdot}{|\cdot|}$ and μ_0 is the air magnetic permeability. In (7), we highlighted the "modulus" of the field - dependent on the EPM-workspace distance ($|r_i|$) and EPM magnetic dipole strength $|\mu_i|$ - and "direction" of the field - related to the direction of the ith EPM to the workspace ($\hat{r}_i$) and EPM orientation ($\hat{\mu}_i$). It should also be noted that (7) is linear with respect to the EPM dipole moment (μ_i) and that the modulus of the EPMs' dipole moment ($|\mu_i|$) is constant.

The gradients of the field with respect to the EPM-workspace relative position (r_i) results into

$$\begin{aligned} \frac{\partial B_i(r_i, \mu_i)}{\partial r_i} &= \mathrm{d}B_i^*(r_i, \mu_i) \\ &= \frac{3\mu_0 |\mu_i|}{4\pi |r_i|^4} \left(\left(I - 5\hat{r}_i \hat{r}_i^T\right)\left(\hat{r}_i^T \hat{\mu}_i\right)\right. \\ &\quad \left. + \hat{\mu}_i \hat{r}_i^T + \hat{r}_i \hat{\mu}_i^T\right). \end{aligned} \tag{8}$$

We parameterize the magnetic dipole of the ith EPM through its orientation with respect to the world frame $\mathcal{W}$. Specifically, we consider the ith EPM reference frame $\mathcal{E}_i$ such that ${}^{\mathcal{E}_i}\mu_i = ||\mu_i|| e_1$. Notice that the orientation of the other axes is arbitrary, since the field is invariant to any rotation around μ_i. In world frame $\mathcal{W}$, the magnetic dipole $\mu_i \equiv {}^{\mathcal{W}}\mu_i = {}^{\mathcal{W}}R_{\mathcal{E}_i}\ {}^{\mathcal{E}_i}\mu_i = R_{\mu_i}(\theta_i, \phi_i) e_1$; here θ_i and ϕ_i are the respective pitch and yaw of the ith EPM. Specifically, $R_{\mu_i}(\theta_i, \phi_i) = \text{rot}_{e_2}(\theta_i)\text{rot}_{e_3}(\phi_i)$, with $\text{rot}_{e_j}(\cdot)$ elementary rotation around the axis e_j.

The position of each EPM is described in polar coordinates $r_i = \rho_i R_{r_i}(\psi_i, \gamma_i) e_1 = ||r_i|| \text{rot}_{e_1}(\psi_i)\text{rot}_{e_3}(\gamma_i) e_1$.

We define the field and independent gradients generated by the ith EPM in the origin of the world frame $\mathcal{W}$ as

$$U_i(\rho_i, \psi_i, \gamma_i, \theta_i, \phi_i) = \begin{pmatrix} B_i^T(r_i, \mu_i) \\ \mathrm{d}B_i^T(r_i, \mu_i) \end{pmatrix}_{\substack{\mu_i = R_{\mu_i}(\theta_i, \phi_i) e_1 \\ r_i = \rho_i R_{r_i}(\psi_i, \gamma_i) e_1}}.$$

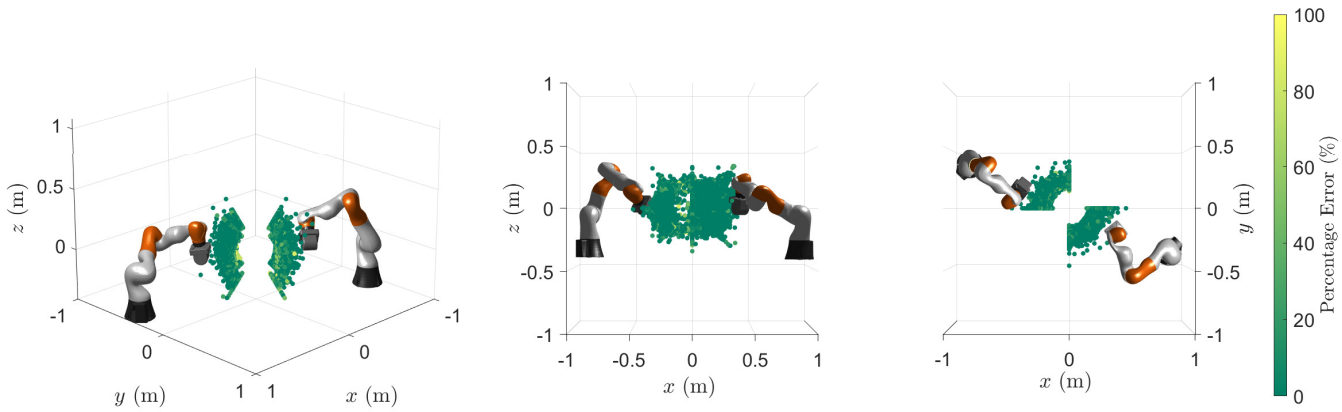

Fig. 2: Optimal solution with polar and kinematic constraints; representation of the percentage error in norm, on the actuated fields and gradients, for each EPM position.

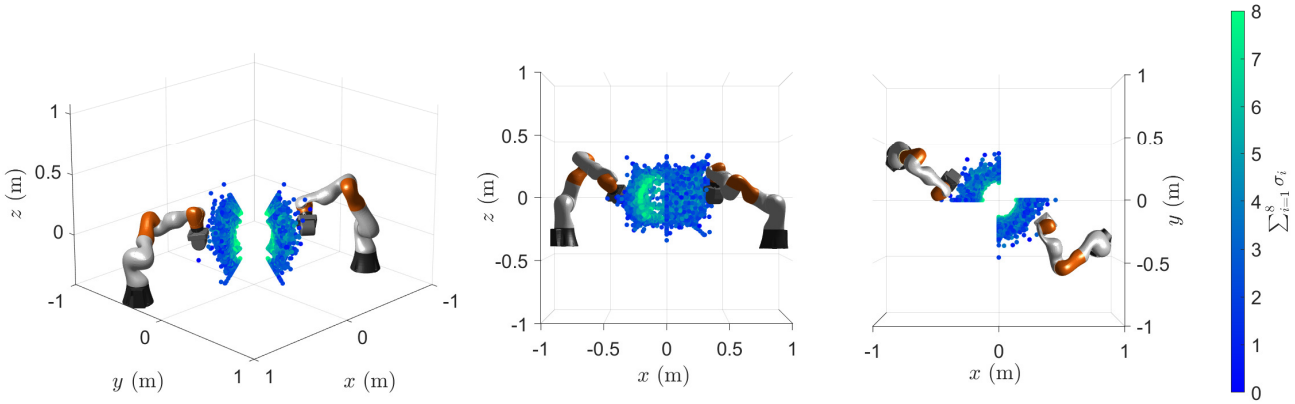

Fig. 3: Representation of the magnetic reach throughout the workspace, i.e. the magnetic DOFs that can be reached from each EPMs' pose via linear motion.

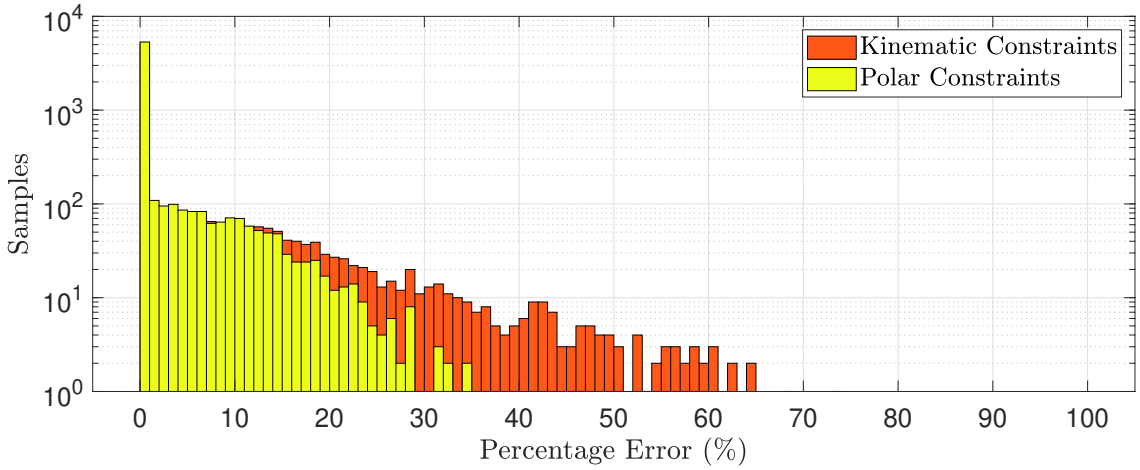

Fig. 4: Representation of samples associated to each error percentage bin of 1%. Error in solving the optimization in (9) over grid of 3^8 combinations of desired field and gradients at discrete levels (0, max/2 and max); maximum field (max=) 10 mT and maximum gradient (max =) 50 mT/m.

The overall field and gradient in the origin of the world frame $\mathcal{W}$ can be written as

$$U = \sum_{i=1}^{2} U_i(\rho_i, \psi_i, \gamma_i, \theta_i, \phi_i),$$

according to the superimposition principle.

We define the state space vector $\chi = (\rho_1 \ \psi_1 \ \gamma_1 \ \theta_1 \ \phi_1 \ \rho_2 \ \psi_2 \ \gamma_2 \ \theta_2 \ \phi_2)^T$ and find the pose of the EPMs, by solving the optimization problem

$$\underset{\chi}{\text{argmin}} ||U_d - U(\chi)||^2 \tag{9}$$

subject to the set of linear constraints

$$\begin{cases} \rho_i > \rho \ \forall \ i \\ \gamma_i \in [\gamma_{min}, \gamma_{max}] \\ \psi_1 \in [\psi_{min}, \psi_{max}] \\ \psi_2 \in [\psi_{min}, \psi_{max}] \, . \end{cases}$$

The polar limits were selected as a linear representation in polar space of the manipulators' reach. This is done in order to reduce the complexity of the error function compared with calculating the full inverse kinematic and checking against the joint space constraints at each sample point. For any desired field and gradients U_d, the minimum radius ρ was imposed to guarantee the EPMs would not exceed safety limits. Table I specifies the parameters selected.

TABLE I: Optimization parameters ($\sim$ unconstrained, $i = 1, 2$)

	ρ_i (m)	ψ_1	ψ_2	γ_i	θ_i	ϕ_i
χ_0	0.35	$-\pi/4$	$\pi/4$	0	0	0
χ_{max}	0.5	0	$\pi/2$	$\pi/4$	$\sim$	$\sim$
χ_{min}	0.2	$-\pi/2$	0	-$\pi/4$	$\sim$	$\sim$

The optimization problem is solved by least squares optimization utilising the "Levenberg–Marquardt" algorithm. For an initial start point for the optimization an initial start state χ_0 is utilised as a guess. This state is chosen as the central point within the linear constraints. In the case that the algorithm fails to converge below the maximum permissible norm error (e_{max}) then the algorithm is reinitialised with a random start state selected uniformly from within the linear constraints. This processed is repeated for a maximum of N random restarts. Once a solution has been found in polar space, standard inverse kinematic solvers are utilised in order to obtain the joint state solution for the collaborative manipulators. Initial state for the inverse kinematics solver is provided by a random configuration from the KUKA robot constraints (See Table II).

TABLE II: Inverse kinematic solver parameters for dual seven axes collaborative manipulators ($i = 1, 2$).

Joints	j_1	j_2	j_3	j_4	j_5	j_6	j_7
q_{max}	170º	120º	170º	120º	170º	120º	175º
q_{min}	-170º	-120º	-170º	-120º	-170º	-120º	-175º

TABLE III: Base position of robots relative to workspace and angular offset around the z axis.

Robots	x (m)	y (m)	z (m)	Angular offset
Robot 1	0.88	-0.38	-0.42	-135^o
Robot 2	-0.88	0.38	-0.42	45^o

In Fig. 2 we report the results for $\rho = 0.2$ m, by generating all the combinations of positive field and gradients up to a maximum, for cylindrical EPMs with dipole moment norm 970.1 Am^2. Specifically, we impose a maximum of (max =) 10 mT for fields and (max =) 50 mT/m for gradients; these were found to be the maximum values we can actuate while satisfying the imposed constraints. For each of the eight DOFs, we sample at three discrete levels (0, max/2 and max) and solve for all the 3^8 combinations. We imposed error tolerance of $e_{max} = 10^{-10}$ and $N = 5$. The error reported in Fig. 2 is the optimization target.

Fig. 2 underlines the position of the EPMs for all the combinations and highlights the error for each desired field and gradients after the kinematics is inverted, i.e. once the kinematic limits were introduced. We show that the robots can reach each individual configuration with minimal error, thus, all the desired DOFs can be guaranteed.

In contrast to coil-based actuation, where the current-to-field mapping is linear, robotically-actuated permanent magnets present a more complex pose-to-field relationship where linear motions do not necessarily result in linear field changes. To understand this relationship within the actuation workspace, we consider the number of positive singular values of the Jacobian matrix $\frac{\partial U}{\partial \chi}$; $\sigma_i = \lambda_i > 0$, with λ ith singular value as a measure of the *magnetic reach* from a specific pose. This represents the number of magnetic DOFs that can be reached from a given configuration of the EPMs through small linear motion of the EPMs themselves. Fig. 3 shows the magnetic reach for the set of poses considered in Fig. 2. It is apparent from Fig. 3 that regions closer to the center of the workspace show high magnetic reach, indicating multiple configurations can be guaranteed through small linear motions. Conversely, at the borders of the workspace, we see reduced magnetic reach, meaning that linear motion does not translate into linear field change and undesirable fields may occur during linear transitions.

Fig. 4 shows how the error is less than 1% for the majority of field and gradient combinations (81.1%), before robots' kinematics is considered. We also notice that applying kinematic constraints minimally impacts the solutions, leading to 76.6% of the error being less than 1%.

The main limiting factor in achieving full convergence is the need for safety constraints. In fact, for some desired gradients, the optimal is achieved when the EPMs are too close to each other. Without constraints, we notice that, in 9.6% of the cases, the robots are closer than 0.2 m, which would apply a load beyond the maximum payload limit for the robots. For this reason, some of the solutions are suboptimal, but safe in terms of EPM-EPM interaction.

V. Experimental Analysis

We perform two sets of experiments to characterize the dEPM platform. Firstly, we demonstrate multi-DOF magnetic actuation (Section V-A), i.e. the ability to control multiple components of fields and gradients independently (measured by means of a teslameter) and multi-DOF magneto-mechanical manipulation (Section V-B) to validate how multi-DOF magnetic actuation can guarantee mechanical actuation of two independent magnets (measured via two six axes load cells). The experimental setup is reported in Fig. 5.

For the first experiment (see Fig. 5a), a teslameter was placed in between the robots and its tip - the sensing portion - localized with respect to the base of each robot (${}^{\mathcal{B}_i}T_{\mathcal{E}_i}, i = 1, 2$) using a four-camera optical tracking system (OptiTrack, NaturalPoint, Inc., USA). For the second set of experiments, described in Fig. 5b, we fixed two IPMs onto two load cells in a vertical rig; we can track the central point between the IPMs by means of the optical tracker and calibrate the system as for the teslameter.

All experiments rely on knowing the pose of the base of each robot with respect to the center of the workspace. For the presented experiments, this was achieved using an optical tracking system shown in Fig. 5, however, for a clinical scenario this may be replaced with an alternative localization system (e.g. electromagnetic [30]) or intraoperative imaging (e.g. fluoroscopy). Optical markers were placed on the end-effector of each robot as well as on the instrument in question (teslameter and load cells mount) with the function of world frame ($\mathcal{W}$). The optical tracker provides the position and rotation of each object with respect to its own reference frame $\mathcal{O}$, in the form ${}^{\mathcal{O}}T_{\mathcal{E}_i} \in \mathrm{SE}(3), i = 1, 2$ and ${}^{\mathcal{O}}T_{\mathcal{W}} \in \mathrm{SE}(3)$, for the respective pose of each EPM and world frame. Thus, using the optical tracker we can obtain the pose of the end-effector of the ith robot in world frame: ${}^{\mathcal{W}}T_{\mathcal{E}_i} = {}^{\mathcal{O}}T_{\mathcal{W}}^{-1}{}^{\mathcal{O}}T_{\mathcal{E}_i}$.

Using direct kinematics, we find the transformation between the base of robot i and its end-effector ${}^{\mathcal{B}_i}T_{\mathcal{E}_i}$; the position of the base of each robot with respect to the world frame was thus found as

$$ {}^{\mathcal{W}}T_{\mathcal{B}_i} = {}^{\mathcal{W}}T_{\mathcal{E}_i}{}^{\mathcal{B}_i}T_{\mathcal{E}_i}^{-1}. $$

This was employed in the control of each robot using the optimization described in Section IV.

The distance between the EPMs was also always controlled to guarantee negligible attraction/repulsion. The maximum safe field and gradients controllable with the system are 200 mT and 500 mT/m respectively; beyond this, the EPM-EPM torque is close to the maximum payload of the robots (EPM-EPM distance of 0.2 m).

A. Magnetic Field Actuation

To validate the multi-DOF magnetic manipulation capabilities of the proposed platform, we measured the generated field using a 3-axial teslameter (AS-N3DM, Projekt Elektronik GmbH, Berlin), represented in Fig. 5a. The robots were controlled as described in Section IV, where the world frame is the tip of the teslameter. We performed eight experiments, controlling the robots to each of the three independently controllable fields and five gradients. In order to compute the gradients in each direction, we varied the position of the world frame origin p_0 in discrete steps, such that the field could be measured along each axis

$$ p_0(T) = \begin{cases} dTe_1 & T \in [0, 5] \\ -d(T-6)e_1 & T \in [6, 10] \\ d(T-12)e_2 & T \in [11, 16] \\ -d(T-16)e_2 & T \in [17, 21] \\ d(T-21)e_3 & T \in [21, 25] \\ -d(T-26)e_3 & T \in [26, 30] \end{cases}, $$

with $d = 0.01$ m, for an overall workspace of $0.1{\times}0.1{\times}0.1$ m^3. By measuring the field along each axis, it was possible to compute the numerical derivative of the field in each direction and measure every component of the gradients. For more details on these experiments, see the Supplementary Video no. 1.

We controlled the field and gradients to values for which we can obtain a large operative workspace, i.e. feasible for general medical applications. We imposed a minimum EPM-EPM distance of 0.5 m and targeted a maximum applied field of 10 mT and gradients between 50 mT/m. Since these experiments require suitable sideways motion of the EPMs for the numerical derivative to be computed, we could not have the EPMs too close to the workspace. In Table IV and V we report the results obtained for all the eight DOFs, when controlled to its positive and negative maximum values, respectively. The *cross talk* is the measure of the amount of activation of the DOFs which are controlled to 0 (off-diagonal elements); it was measured as the mean for each trial (row of Table IV and V).

Since we assume linear fields (or constant gradients), for each trial, we computed how much the measured field differs from the ideal linear field

$$ B_d(T) = B_d(0) + \mathrm{d}B_d^* \; p_0(T). $$

For each measured field $B_m(T)$, we compute the max absolute error

$$ \max_T ||B_d(T) - B_m(T)||, $$

which is reported in Table IV and V as the *linear error* ("Lin. err.").

Overall, the experiments demonstrate that the approximation of constant gradients holds, given the limited errors with respect to linear fields (maximum 9.2%). The maximum experienced cross talk is 17.2%, which is acceptable in open-loop. The mean error with respect to desired set-point is 13.5% on the field and gradient actuation (i.e. the one on the diagonal components of Table IV and V). These results highlight that the optimization technique discussed in Section IV is able to accurately control eight independent magnetic DOFs. We expect closed loop control will further reduce errors and cross talk.

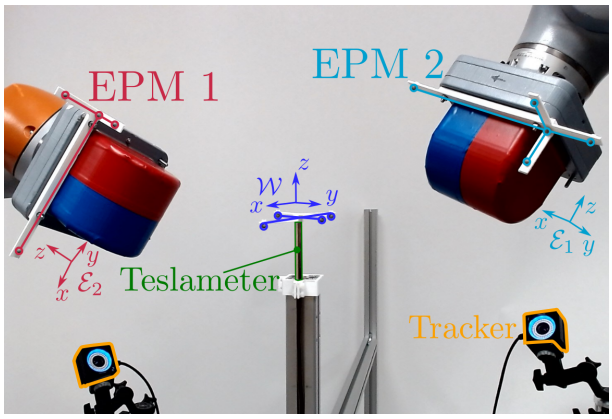

(a) Teslameter experiments.

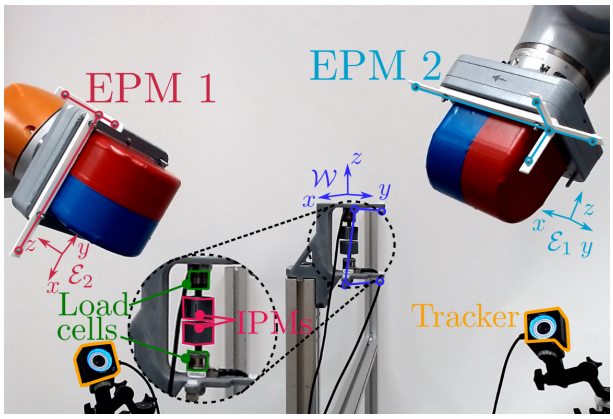

(b) Load cell experiments.

Fig. 5: Experimental setup utilized for (a) characterization of the magnetic field and field gradients within the workspace using a teslameter, and (b) magneto-mechanical manipulation using two orthogonal IPMs

TABLE IV: Summary of the data from teslameter: field in center of the workspace and numerical derivatives along each axis. *Positive* field (mT) and gradients (mT/m). Desired field is 10 mT and gradient 50 mT/m along the diagonal; 0 is desired for the off-diagonal elements.

	Case								**Accuracy**	
	Bx	By	Bz	$\frac{\partial Bx}{\partial x}$	$\frac{\partial Bx}{\partial y}$	$\frac{\partial Bx}{\partial z}$	$\frac{\partial By}{\partial y}$	$\frac{\partial By}{\partial z}$	Cross talk (%)	Lin. err. (%)
B_1	**9.6**	-0.2	-0.25	11.5	5.1	14	-4.1	0.5	10.7	3.7
B_2	0.4	**9.2**	1.1	-2.9	-0.3	3.9	-12.1	13.7	11.6	3.5
B_3	1.8	-2.0	**9.4**	-10.7	13.9	10.5	-2.0	13.7	19.9	8.0
$\mathrm{d}B_1$	0.1	-0.0	0.7	**35.1**	-0.1	-4.1	-1.2	-1.5	4.5	0.6
$\mathrm{d}B_2$	-0.15	0.4	0.2	0.8	**45.3**	-4.4	-2.3	-2.8	4.0	0.9
$\mathrm{d}B_3$	-0.8	0.0	0.2	7.4	0.8	**39.1**	-3.6	-2.3	8.9	0.8
$\mathrm{d}B_4$	0.1	-0.2	0.9	6.9	4.5	-0.3	**47.4**	9.6	9.7	0.7
$\mathrm{d}B_5$	0.0	-0.7	-0.2	-0.1	1.6	-1.2	-11.3	**35.9**	6.4	0.8

TABLE V: Summary of the data from teslameter: field in center of the workspace and numerical derivatives along each axis. *Negative* field (mT) and gradients (mT/m). Desired field is -10 mT and gradient -50 mT/m along the diagonal; 0 is desired for the off-diagonal elements.

	Case								**Accuracy**	
	Bx	By	Bz	$\frac{\partial Bx}{\partial x}$	$\frac{\partial Bx}{\partial y}$	$\frac{\partial Bx}{\partial z}$	$\frac{\partial By}{\partial y}$	$\frac{\partial By}{\partial z}$	Cross talk (%)	Lin. err. (%)
B_1	**-9.9**	0.2	0.0	-10.1	-2.6	-13.8	3.9	1.1	9.3	9.2
B_2	-0.5	**-9.1**	-1.4	0.1	1.8	3.1	11.3	-13.9	11.5	6.0
B_3	-2.3	2.2	**-9.8**	9.6	-4.2	-8.9	1.0	13.8	17.2	5.2
$\mathrm{d}B_1$	-0.1	0.02	-1.1	**-42.4**	-3.5	4.9	0.5	-0.5	4.5	0.8
$\mathrm{d}B_2$	0.1	-0.2	-0.2	-4.3	**-42.7**	1.0	0.5	0.84	2.7	0.5
$\mathrm{d}B_3$	0.5	0.1	-0.4	-9.4	1.3	**-38.7**	2.7	-0.1	5.2	0.5
$\mathrm{d}B_4$	-0.2	-0.1	-0.81	-1.4	1.0	0.9	**-41.6**	-11.2	5.8	2.7
$\mathrm{d}B_5$	0.0	0.5	-0.1	0.2	-1.8	-1.1	3.5	**-38.6**	2.7	0.5

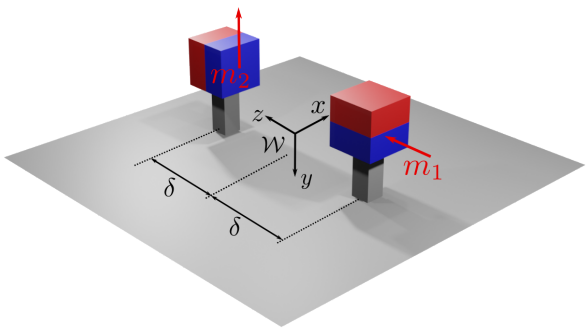

Fig. 6: Schematic representation of the magneto-mechanical experiments.

B. Magneto-Mechanical Manipulation

In the following, we describe how the independent magnetic DOFs, analysed in the previous section, can be used to actuate two independent permanent magnets. This results would also apply to other objects exhibiting magnetic behaviour, such as coils or magnetic particles embedded in soft polymers [31]. The scenario is schematically represented in Fig. 6. We positioned two orthogonally-magnetized IPMs along the global z axis, spaced at a distance $\delta = 9.5$ mm from the center of the world reference frame ($\mathcal{W}$). The magnets, $9.5 \times 9.5 \times 9.5$ mm^3 grade N-42 (K&J Magnetics, Inc., USA), were aligned so that their magnetic dipole was along z, $\hat{m}_1 = e_3$ and y, $\hat{m}_2 = -e_2$; here, $||m_1|| = ||m_2|| = ||m||$

By applying (3), the wrench on each IPM can be computed as

$$w_1 = ||m|| \begin{pmatrix} \mathrm{d}B_3 \\ \mathrm{d}B_5 \\ -\mathrm{d}B_1 - \mathrm{d}B_4 \\ -B_2 - \delta \mathrm{d}B_5 \\ B_1 + \delta \mathrm{d}B_3 \\ 0 \end{pmatrix}$$

$$w_2 = ||m|| \begin{pmatrix} -\mathrm{d}B_2 \\ -\mathrm{d}B_4 \\ -\mathrm{d}B_5 \\ -B_3 - \delta(\mathrm{d}B_1 + \mathrm{d}B_4) \\ 0 \\ B_1 - \delta \mathrm{d}B_3 \end{pmatrix}.$$

We assume $\delta \approx 0$ and select the independent DOFs to actuate

$$w = \begin{pmatrix} w_{1_1} \\ w_{1_2} \\ w_{1_3} \\ w_{1_1} \\ w_{1_2} \\ w_{2_1} \\ w_{2_2} \\ w_{2_1} \end{pmatrix} = \begin{pmatrix} f_{1_x} \\ f_{1_y} \\ f_{1_z} \\ \tau_{1_x} \\ \tau_{1_y} \\ f_{2_x} \\ f_{2_y} \\ \tau_{2_x} \end{pmatrix} = ||m|| \begin{pmatrix} \mathrm{d}B_3 \\ \mathrm{d}B_5 \\ -\mathrm{d}B_1 - \mathrm{d}B_4 \\ -B_2 \\ B_1 \\ -\mathrm{d}B_2 \\ -\mathrm{d}B_4 \\ -B_3 \end{pmatrix}$$

These DOFs can be independently manipulated using our actuation system. To demonstrate this, we controlled the field and gradient components to the same maximum values of the previous experiments.

We performed these experiments with the setup shown in Fig. 5b. The wrench on each IPM was measured with a six-axes load cell (Nano 17, ATI Industrial Automation, USA) with 6.25 mN and 31.25 mN·m resolution in force and torque, respectively. The load cell readings were zeroed before each experiment to offset the IPM-IPM interaction. Since the IPMs are not able of relative motion, the zeroing applies to the entire data acquisition.

The results for positive and negative wrenches are reported in Fig. 7. In figure, we show the activation of each independent DOF, as we control them in a pre-computed sequence of EPMs positions. We selected the eight independent DOFs and computed the EPMs pose by applying the optimization described in Section IV. The y-axis represents the amount of activation of each independent force and torque, in their respective units. The torque is reported in N·mm and the force in cN (10^{-2} N) to be comparable in the figures. For more details on the experiments, see the Supplementary Video no. 2.

The data shows minimal cross talk and demonstrates that all the target DOFs can be actuated independently in open-loop. We built the time-series $T = (T_1, T_2, \ldots, T_8)$ where T_i is the time where the ith DOF activates. To compute the cross talk, we find the mean cross-activation of the of the ith DOF (DOF$_i$) as

$$\alpha_i = \frac{1}{7} \sum_{j \neq i} \mathrm{DOF}_i(T_j),$$

i.e. the activation when it is desired not to be active. Its activation, when controlled to its maximum, is $A_i = \mathrm{DOF}_i(T_i)$. We measure the percentage mean cross talk as $100 \cdot A_i/\alpha_i$ and report the results in Table VI.

We can see that the worst-case mean cross talk is as small as 6.1% which demonstrates that up to eight DOFs can be actuated independently. We also notice that the assumption of small δ is satisfied, since the application of gradients (forces) does not generate undesired torques. The mean error with respect to the prediction from the dipole model is 10.85% and 11.10% in the respective positive and negative case, which is comparable to what experienced with field measurements (Table IV and V).

Compared to coil-based actuation, the transition between independent DOFs is not inherently smooth when the robots

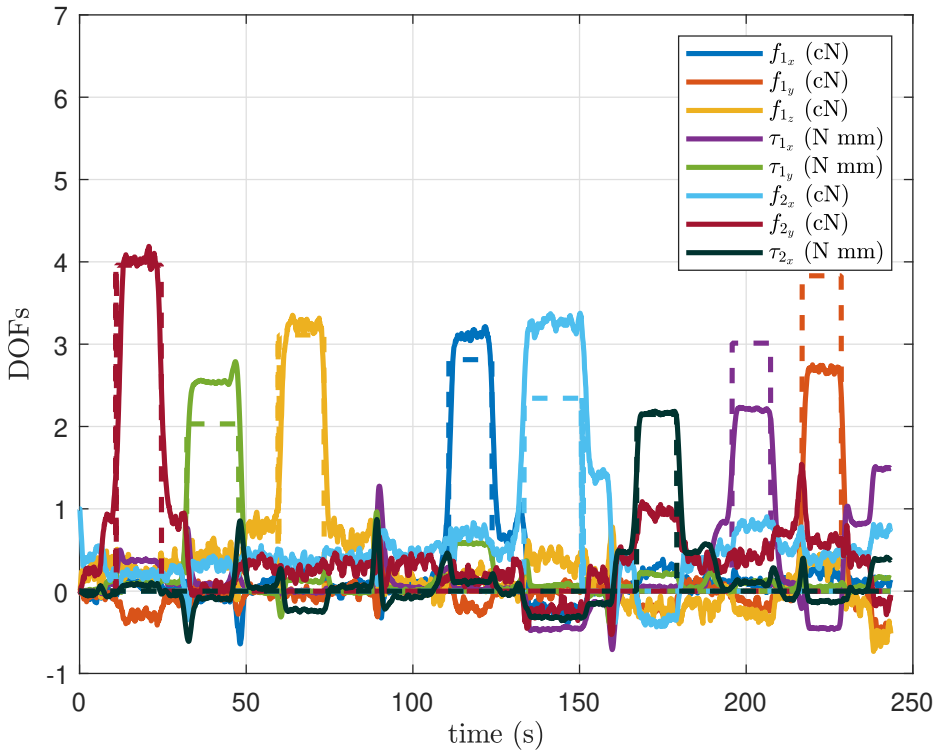

(a) Positive wrench.

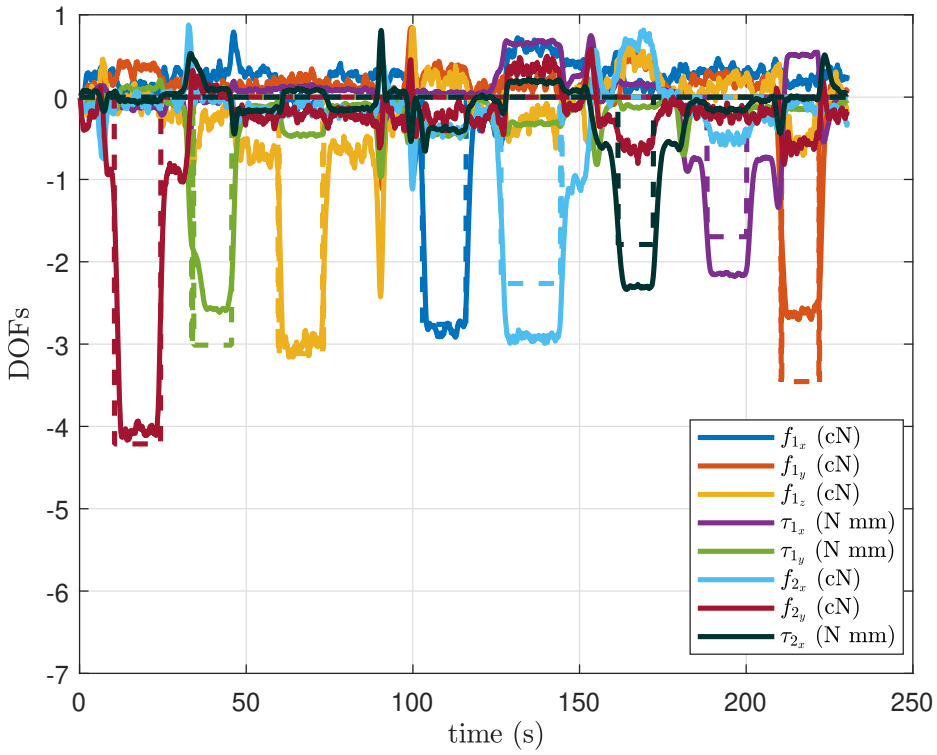

(b) Negative wrench.

Fig. 7: Results of the magneto-mechanical experiments. Dashed lines indicates the dipole model prediction and solid line the measured data.

TABLE VI: Mean cross talk of the magneto-mechanical DOFs in percentage.

DOF	1	2	3	4	5	6	7	8
Positive	0.8	0.7	1.2	1.3	1.0	3.9	1.4	1.0
Negative	6.1	4.9	0.9	2.5	0.9	0.6	0.7	2.2

are controlled in a point-to-point fashion. In fact, this approach does not guaranteed that the transition is linear and it may generate undesired transient behaviours. This can be mitigated by introducing appropriate path planning for the robots' motion.

VI. Conclusion

In the present work, we introduced a novel approach for multi-DOF magnetic actuation in magneto-mechanical robot manipulation. We discussed how this can be achieved by using a dual permanent magnet approach, with the EPMs being collaboratively actuated by two independent serial manipulators. We show that the introduced dEPM platform can both control gradient-free fields in all three directions and five main independent gradients components.

We demonstrate that a least-squares optimization routine can find the pose of the EPMs for a consistent set of combinations of every field and gradient. The solution is found within safety constraints, i.e. the EPMs are imposed not to invade a reserved workspace. We also consider the effect of the kinematic constraints of the robots and prove that a seven axes manipulator is able to accurately control the EPMs to the desired poses.

We validate our claims with multiple experiments. Firstly, we measure the fields and gradients in a 10^3 cm^3 workspace with EPMs at a distance of 50 cm to one another, by means of a teslameter. We prove that both the desired gradient-free field and gradients can be generated independently. The distance between the robots is compatible with medical applications, since the workspace is large enough to fit a patient.

We then prove how the applied field and gradients can be used for mechanical actuation by measuring the wrench on two separated magnets via a pair of six-axes load cells. We constrain the motion of the robots to a safe area and prove that eight mechanical DOFs can be actuated in this case. In the worst-case scenario, we record a mean cross talk of 6.1% in open loop. During the experiment, the EPMs were controlled to move in a point-to-point fashion, which leads to possible spikes in the measured wrench. In the future, we will investigate smoothing of the applied wrench via optimal planning of the EPMs motion.

Herein, we prove that the dEPM platform is capable of achieving similar levels of magnetic manipulability to what can be obtained with system of coils [5], [6]. We expect that the proposed actuation system can introduce a novel approach in remote actuation of small medical devices, which can generate stronger fields in a larger workspace compared to its coil-based counterpart.

Utilizing the dual EPM system within specific applications will necessitate consideration of the IPMs interaction forces and associated mechanical constraints of the robot's design. The associated force and torque requirements will determine suitability of the system, however, to minimize instabilities caused by IPMs cross talk and non-linear transitions, we will investigate closed-loop control, robots path planning and improved modelling of the field. Further, application to medical diagnosis and treatment will be analysed with the aim of applying the actuation system to large scale anatomy [31]. In these cases, the large fields and workspace, combined with the magnetic manipulability here demonstrated, will play a fundamental role in enabling navigation of complex anatomical structures.

References

[1] J. Edelmann, A. J. Petruska, and B. J. Nelson, "Estimation-Based Control of a Magnetic Endoscope without Device Localization," *Journal of Medical Robotics Research*, vol. 03, no. 01, p. 1850002, 2018.

[2] A. Hong, A. J. Petruska, A. Zemmar, and B. J. Nelson, "Magnetic Control of a Flexible Needle in Neurosurgery," *IEEE Transactions on Biomedical Engineering*, vol. 68, no. 2, pp. 616–627, 2021.

[3] T. L. Bruns, K. E. Riojas, D. S. Ropella, M. S. Cavilla, A. J. Petruska, M. H. Freeman, R. F. Labadie, J. J. Abbott, and R. J. Webster, "Magnetically Steered Robotic Insertion of Cochlear-Implant Electrode Arrays: System Integration and First-In-Cadaver Results," *IEEE Robotics and Automation Letters*, vol. 5, no. 2, pp. 2240–2247, 2020.

[4] M. C. Hoang, K. T. Nguyen, V. H. Le, J. Kim, E. Choi, B. Kang, J. O. Park, and C. S. Kim, "Independent Electromagnetic Field Control for Practical Approach to Actively Locomotive Wireless Capsule Endoscope," *IEEE Transactions on Systems, Man, and Cybernetics: Systems*, vol. 51, no. 5, pp. 3040–3052, 2021.

[5] S. Salmanipour and E. Diller, "Eight-Degrees-of-Freedom Remote Actuation of Small Magnetic Mechanisms," in *2018 IEEE International Conference on Robotics and Automation (ICRA)*, 2018, pp. 3608–3613.

[6] S. Salmanipour, O. Youssefi, and E. D. Diller, "Design of Multi-Degrees-of-Freedom Microrobots Driven by Homogeneous Quasi-Static Magnetic Fields," *IEEE Transactions on Robotics*, vol. 37, no. 1, pp. 246–256, 2021.

[7] M. Richter, V. K. Venkiteswaran, and S. Misra, "Multi-Point Orientation Control of Discretely-Magnetized Continuum Manipulators," *IEEE Robotics and Automation Letters*, vol. 6, no. 2, pp. 3607–3614, 2021.

[8] Z. Yang, L. Yang, M. Zhang, Q. Wang, S. C. H. Yu, and L. Zhang, "Magnetic Control of a Steerable Guidewire Under Ultrasound Guidance Using Mobile Electromagnets," *IEEE Robotics and Automation Letters*, vol. 6, no. 2, pp. 1280–1287, 2021.

[9] R. Chen, D. Folio, and A. Ferreira, "Mathematical approach for the design configuration of magnetic system with multiple electromagnets," *Robotics and Autonomous Systems*, vol. 135, p. 103674, 2021.

[10] J. J. Abbott, E. Diller, and A. J. Petruska, "Magnetic Methods in Robotics," *Annual Review of Control, Robotics, and Autonomous Systems*, vol. 3, no. 1, pp. 57–90, may 2020. [Online]. Available: https://doi.org/10.1146/annurev-control-081219-082713

[11] T. da Veiga, J. H. Chandler, P. Lloyd, G. Pittiglio, N. J. Wilkinson, A. K. Hoshiar, R. A. Harris, and P. Valdastri, "Challenges of continuum robots in clinical context: a review," *Progress in Biomedical Engineering*, vol. 2, no. 3, p. 32003, 2020. [Online]. Available: http://dx.doi.org/10.1088/2516-1091/ab9f41

[12] G. Pittiglio, J. H. Chandler, M. Richter, V. K. Venkiteswaran, S. Misra, and P. Valdastri, "Dual-Arm Control for Enhanced Magnetic Manipulation," in *2020 IEEE/RSJ International Conference on Intelligent Robots and Systems (IROS)*, 2020, pp. 7211–7218.

[13] G. Pittiglio, L. Barducci, J. W. Martin, J. C. Norton, C. A. Avizzano, K. L. Obstein, and P. Valdastri, "Magnetic Levitation for Soft-Tethered Capsule Colonoscopy Actuated With a Single Permanent Magnet: A Dynamic Control Approach," *IEEE Robotics and Automation Letters*, vol. 4, no. 2, pp. 1224–1231, 2019.

[14] M. Yousefi and H. Nejat Pishkenari, "Independent position control of two identical magnetic microrobots in a plane using rotating permanent magnets," *Journal of Micro-Bio Robotics*, vol. 17, no. 1, pp. 59–67, 2021. [Online]. Available: https://doi.org/10.1007/s12213-021-00143-w

[15] J. Sikorski, I. Dawson, A. Denasi, E. E. Hekman, and S. Misra, "Introducing BigMag - A novel system for 3D magnetic actuation of flexible surgical manipulators," *Proceedings - IEEE International Conference on Robotics and Automation*, pp. 3594–3599, 2017.

[16] P. Ryan and E. Diller, "Magnetic actuation for full dexterity microrobotic control using rotating permanent magnets," *IEEE Transactions on Robotics*, vol. 33, no. 6, pp. 1398–1409, 2017.

[17] F. Carpi and C. Pappone, "Stereotaxis Niobe® magnetic navigation system for endocardial catheter ablation and gastrointestinal capsule endoscopy," *Expert review of medical devices*, vol. 6, no. 5, pp. 487–498, 2009.

[18] A. J. Petruska, J. Edelmann, and B. J. Nelson, "Model-Based Calibration for Magnetic Manipulation," *IEEE Transactions on Magnetics*, vol. 53, no. 7, pp. 1–6, 2017.

[19] J. Edelmann, A. J. Petruska, and B. J. Nelson, "Magnetic control of continuum devices," *International Journal of Robotics Research*, vol. 36, no. 1, pp. 68–85, 2017.

[20] Magnetecs, "Magnetecs: Guiding Medical Technology," http://www.magnetecs.com/overview.php, 2021.

[21] K. Mandal, F. Parent, S. Martel, R. Kashyap, and S. Kadoury, "Vessel-based registration of an optical shape sensing catheter for MR navigation," *International Journal of Computer Assisted Radiology and Surgery*, vol. 11, no. 6, pp. 1025–1034, 2016. [Online]. Available: https://doi.org/10.1007/s11548-016-1366-7

[22] I. Tunay, "Position control of catheters using magnetic fields," in *Proceedings of the IEEE International Conference on Mechatronics, 2004. ICM '04.*, 2004, pp. 392–397.

[23] ——, "Modeling magnetic catheters in external fields," in *The 26th Annual International Conference of the IEEE Engineering in Medicine and Biology Society*, vol. 1, 2004, pp. 2006–2009.

[24] O. Erin, D. Antonelli, M. E. Tiryaki, and M. Sitti, "Towards 5-DoF Control of an Untethered Magnetic Millirobot via MRI Gradient Coils," in *2020 IEEE International Conference on Robotics and Automation (ICRA)*, 2020, pp. 6551–6557.

[25] O. Erin, C. Alici, and M. Sitti, "Design, Actuation, and Control of an MRI-Powered Untethered Robot for Wireless Capsule Endoscopy," *IEEE Robotics and Automation Letters*, vol. 6, no. 3, pp. 6000–6007, 2021.

[26] A. Azizi, C. C. Tremblay, K. Gagné, and S. Martel, "Using the fringe field of a clinical MRI scanner enables robotic navigation of tethered instruments in deeper vascular regions," *Science Robotics*, vol. 4, no. 36, p. eaax7342, 2019. [Online]. Available: http://robotics.sciencemag.org/content/4/36/eaax7342.abstract

[27] D. Lin, N. Jiao, Z. Wang, and L. Liu, "A Magnetic Continuum Robot With Multi-Mode Control Using Opposite-Magnetized Magnets," *IEEE Robotics and Automation Letters*, vol. 6, no. 2, pp. 2485–2492, 2021.

[28] A. J. Petruska and J. J. Abbott, "Optimal Permanent-Magnet Geometries for Dipole Field Approximation," *IEEE Transactions on Magnetics*, vol. 49, no. 2, pp. 811–819, 2013.

[29] A. J. Petruska and B. J. Nelson, "Minimum bounds on the number of electromagnets required for remote magnetic manipulation," *IEEE Transactions on Robotics*, vol. 31, no. 3, pp. 714–722, 2015.

[30] A. Z. Taddese, P. R. Slawinski, M. Pirotta, E. De Momi, K. L. Obstein, and P. Valdastri, "Enhanced real-time pose estimation for closed-loop robotic manipulation of magnetically actuated capsule endoscopes," *The International journal of robotics research*, vol. 37, no. 8, pp. 890–911, 2018.

[31] G. Pittiglio, P. Lloyd, T. da Veiga, O. Onaizah, C. Pompili, J. H. Chandler, and P. Valdastri, "Patient-specific magnetic catheters for atraumatic autonomous endoscopy," *Soft Robotics*, vol. 0, no. 0, p. null, 0, pMID: 35312350. [Online]. Available: https://doi.org/10.1089/soro.2021.0090